

Article

Optimal Scheduling of Virtual Power Plant Considering Reconfiguration of District Heating Network

Jinhao Wang ¹, Zhaoguang Pan ^{2,*}, Shengwen Li ¹, Huaichang Ge ², Gang Yang ¹ and Bin Wang ²¹ Electric Power Research Institute of State Grid Shanxi Electric Power Company, Taiyuan 030000, China² Department of Electrical Engineering, Tsinghua University, Beijing 100084, China

* Correspondence: panzg09@163.com

Abstract: A combined heat and power virtual power plant (CHP-VPP) can effectively control the distributed resources in an electric–thermal coupling system and solve the problem of lack of flexibility caused by large-scale renewable energy grid connection. Similar to the optimal reconfiguration of distribution network topology by operating switches, the district heating system is also equipped with tie and sectionalizing valves to realize the optimal adjustment of district heating network (DHN) topology, which provides an economical and effective method for improving the power system’s flexibility. Based on this, this paper proposes a CHP-VPP economic scheduling model considering reconfigurable DHN. Firstly, the energy flow model is introduced to reduce the computational complexity. Secondly, adaptive robust optimization solved by the column-and-constraint generation algorithm is used to settle the randomness of wind power to ensure that the results are feasible in all worst scenarios. Finally, the feasibility of the proposed model is illustrated by case studies based on an actual CHP-VPP. The results show that compared with the reference case, considering the reconfigurability of DHN in the CHP-VPP optimization scheduling process can reduce the cost by about 2.78%.

Keywords: virtual power plants; economic scheduling; reconfigurable DHN; adjustable robust optimization



Citation: Wang, J.; Pan, Z.; Li, S.; Ge, H.; Yang, G.; Wang, B. Optimal Scheduling of Virtual Power Plant Considering Reconfiguration of District Heating Network. *Electronics* **2023**, *12*, 3409. <https://doi.org/10.3390/electronics12163409>

Academic Editor: J. C. Hernandez

Received: 10 July 2023

Revised: 29 July 2023

Accepted: 4 August 2023

Published: 11 August 2023



Copyright: © 2023 by the authors. Licensee MDPI, Basel, Switzerland. This article is an open access article distributed under the terms and conditions of the Creative Commons Attribution (CC BY) license (<https://creativecommons.org/licenses/by/4.0/>).

1. Introduction

The world’s energy shortage and environmental pollution have become increasingly serious in recent years, and the deficiencies of traditional energy power generation have been highlighted [1,2]. Renewable energy has become the primary focus of global energy development in the future. By the end of 2021, global renewable energy generation was 3064 GW, an increase of 9.1% compared to 2020 [3]. However, the intermittence and volatility of renewable energy generation lead to potential security risks in the actual operation of the power system, which hinders the further development of renewable energy consumption capacity.

As an important distributed resource technology, virtual power plants (VPPs) provide a solution to improve renewable energy consumption [4,5]. Ref. [6] established an overall economic optimization model of multi-generator units under VPP mode, and the energy storage equipment was used to effectively reduce the rate of ‘abandoning wind and light’. Ref. [7] proposed an operation mode of electric vehicle VPPs participating in the ancillary service market to promote deep peak shaving of heat power and consumption of intermittent renewable energy. Also, researchers noted that uncertainty is a significant factor affecting the operation of VPPs. Robust optimization [8], stochastic optimization [9] and opportunity constraints [10] are popularly used to handle uncertainty.

Meanwhile, with the wide application of electric–thermal coupling components like combined heat and power (CHP) units and electric boilers (EBs), the coupling relationship between electricity and heat has become closer [11,12]. The combined heat and power virtual power plant (CHP-VPP), as a coupling system of electricity and heat, has aroused

the interests of researchers. Ref. [13] studied the financial benefits of heat load management in a CHP-VPP comprising a micro-CHP unit, a heat pump and residential heat storage. Ref. [14] constructed a CHP-VPP cooperative game model based on the improved Sharpley value method.

However, the above studies ignore the district heating network (DHN) model in VPP or assume that the topology of DHN is constant. Similar to the topology reconfiguration of the power distribution network (PDN) by controlling remote switches, the topology of DHN in CHP-VPP can also be reconfigured by distance control pipeline valves [15]. On the one hand, the heat load after reconfiguration can be redistributed between heat sources to obtain a more economical scheduling plan to decrease the cost of the whole system. On the other hand, the operation flexibility of CHP units is enhanced after reconfiguration, and the capacity of renewable energy consumption is also improved. Some researchers have studied the application of reconfigurable DHN in integrated energy systems. Ref. [16] studied the seasonal DHN reconstruction to improve the rationality of the planning strategy. Ref. [17] considered the collaborative reconfiguration of the power distribution system (PDS) and district heating system (DHS) to enhance the flexibility of park-level integrated power and heating systems.

Accordingly, this paper takes a CHP-VPP with wind turbines (WTs), conventional generators, CHP units and EBs as an example to establish an economic dispatch model considering reconfigurable DHN. The following are the contributions of this paper:

- (1) For the first time, the reconfigurable DHN is considered in the economic scheduling problem of CHP-VPP, which can significantly reduce the operating cost of CHP-VPP. The energy flow model is introduced to reduce the difficulty of solving the model.
- (2) Adaptive robust optimization (ARO) solved by the column-and-constraint generation (C&CG) algorithm is applied to settle the randomness of wind power, and in order to avoid too conservative decision-making, a robust control coefficient is introduced for adjustment.
- (3) The effectiveness and versatility of the CHP-VPP economic dispatch model considering reconfigurable DHN are verified by an example analysis based on an actual CHP-VPP in China.

2. Optimal Scheduling Model of CHP-VPP Considering Reconfigurable DHN

Figure 1 presents the internal framework of the CHP-VPP. The electric power is generated by CHP units, WTs and conventional generators. In addition, CHP-VPP can interact with the power grid through tie lines and provide electricity through the PDN. The heat in CHP-VPP is generated by the heating station with a heat source (CHP units and EBs) and transported by the circulating hot water via DHN. The configuration of DHN can be changed by remote control of the pipeline valve.

The CHP-VPP operator schedules all units and pipeline valves of DHN within its jurisdiction based on the principle of maximizing renewable energy power generation. Furthermore, the CHP-VPP, as an independent entity, can participate in electricity trading in the electricity market [18]. At a low electricity price, the CHP-VPP chooses to purchase electricity from the grid, reducing internal power generation to reduce costs; on the contrary, it sells electricity to the grid to increase the revenue.

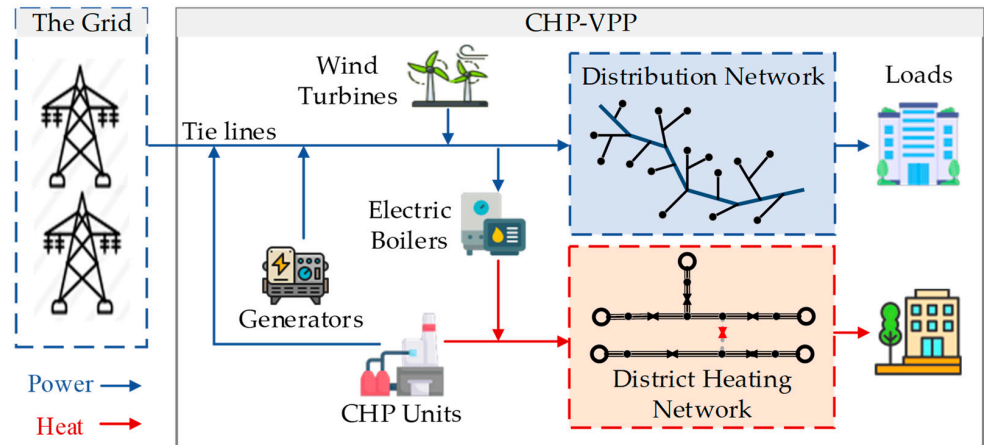


Figure 1. The structure of CHP-VPP.

2.1. Objective Function

The model proposed in our study purposes to minimize the operation cost of the CHP-VPP during the scheduling period.

$$\min C = C^s + C^f + C^e \tag{1}$$

where C^s and C^f are the start-up costs and fuel costs of the units in the CHP-VPP, respectively; C^e is the cost of interacting with the power grid.

2.1.1. Start-Up Costs

Each start-up of the units requires a fixed cost, as follows:

$$C^s = \sum_{i \in I_G \cup I_{CHP}} \sum_{t=1}^{24} \lambda_i^s y_t^i + \sum_{j \in I_{EB}} \sum_{t=1}^{24} \lambda_j^s y_t^j \tag{2}$$

where $\lambda_i^s / \lambda_j^s$ are the start-up cost coefficients of unit i except EB/EB j ; y_t^i / y_t^j are binary variables, which represent the starting state of unit i except EB/EB j ; and I_G , I_{CHP} and I_{EB} represent the set of generators, CHP units and EBs, respectively.

2.1.2. Fuel Costs

The fuel costs are calculated according to the output power of each unit, as shown below:

$$C^f = \sum_{i \in I_G} \sum_{t=1}^{24} \lambda_i^f p_t^i + \sum_{i \in I_{CHP}} \sum_{t=1}^{24} (\lambda_i^e p_t^i + \lambda_i^h h_t^i) \tag{3}$$

where λ_i^f is the fuel cost coefficient of generator i ; λ_i^e and λ_i^h are the electric and heat cost coefficients of CHP i ; and p_t^i and h_t^i are the outputs of active power and heat of unit i , respectively.

2.1.3. Costs of Interacting with the Power Grid

The CHP-VPP chooses to purchase or sell electricity at each time period according to the electricity price.

$$C^e = \sum_{t=1}^{24} (\lambda_t^{sell} x_t^{sell} + \lambda_t^{pur} x_t^{pur}) p_t^e \tag{4}$$

where p_t^e is the power that interacts with the grid. When $p_t^e > 0$, it denotes that the CHP-VPP acquires electricity from the grid; on the contrary, when $p_t^e < 0$, it means the CHP-VPP sells electricity to the grid. λ_t^{sell} and λ_t^{pur} indicate the price of selling and purchasing

electricity at time t . x_t^{sell} and x_t^{pur} are binary variables that indicate the state of CHP selling and purchasing electricity at time t .

2.2. Operation Constraints of PDS

In our study, a DistFlow power flow equation [19] is utilized to construct the active power flow (5), reactive power flow (6) and voltage drop (7) equations of the branch in PDN.

$$\sum_{d \in \pi(j)} P_t^{jd} + \hat{p}_t^{WT,j} + p_t^{CHP,j} + p_t^{G,j} - p_t^{EB,j} - P_t^{EL,j} - P_t^{ij} = 0 \tag{5}$$

$$\sum_{d \in \pi(j)} Q_t^{jd} + \hat{q}_t^{WT,j} + q_t^{CHP,j} + q_t^{G,j} - q_t^{EB,j} - Q_t^{EL,j} - Q_t^{ij} = 0 \tag{6}$$

$$V_t^i - V_t^j = (P_t^{ij} r^{ij} + Q_t^{ij} x^{ij}) / V_t^{base}, \forall t \tag{7}$$

where P_t^{ij} / Q_t^{ij} are the active/reactive power, respectively; V_t^j / V_t^{base} are the voltage/voltage reference values; r^{ij}, x^{ij} are the impedance of branch (i,j) ; $p_t^{CHP,j}, p_t^{G,j}, p_t^{EB,j}, \hat{p}_t^{WT,j}$ represent the active power of the CHP unit/generator/EB/WT connected to node j ; $q_t^{CHP,j}, q_t^{G,j}, q_t^{EB,j}, \hat{q}_t^{WT,j}$ represent the output reactive power of the CHP unit/generator/EB/WT connected to node j ; $P_t^{EL,j} / Q_t^{EL,j}$ are the active/reactive power of electric load; and $\pi(j)$ is the set of children nodes of node j .

Constraint (8) defines the capacity limit of the branch and constraint (9) describes the limit of the node voltage.

$$P_t^{ij,min} \leq P_t^{ij} \leq P_t^{ij,max}, Q_t^{ij,min} \leq Q_t^{ij} \leq Q_t^{ij,max}, \forall t \tag{8}$$

$$V_t^{j,min} \leq V_t^j \leq V_t^{j,max}, \forall t \tag{9}$$

where $P_t^{ij,min} / Q_t^{ij,min}$ are the minimum active/reactive power of branch (i,j) , respectively; $P_t^{ij,max} / Q_t^{ij,max}$ are the maximum active/reactive power of branch (i,j) ; and $V_t^{j,min} / V_t^{j,max}$ are the minimum/maximum voltage value of node j .

Constraint (10) is the power balance equation of the whole CHP-VPP.

$$p_t^G + \hat{p}_t^{WT} + p_t^{CHP} + p_t^e = P_t^{EL} + p_t^{EB}, \forall t \tag{10}$$

Constraints (11) and (12) regulate the start-up operation of all devices. Constraint (13) defines the output range of all units, and the ramping limits are restrained by constraint (14).

$$x_t^i - x_{t-1}^i \leq y_t^i, x_t^j - x_{t-1}^j \leq y_t^j, \forall t, \forall i \in I_G \cup I_{CHP}, \forall j \in \cup I_{EB} \tag{11}$$

$$\sum_{t=1}^{24} y_t^i \leq N^i, \sum_{t=1}^{24} y_t^j \leq N^j, \forall t, \forall i \in I_G \cup I_{CHP}, \forall j \in I_{EB} \tag{12}$$

$$x_t^i P^{i,min} \leq p_t^i \leq x_t^i P^{i,max}, x_t^j P^{j,min} \leq p_t^j \leq x_t^j P^{j,max}, \forall t, \forall i \in I_G \cup I_{CHP}, \forall j \in \cup I_{EB} \tag{13}$$

$$-\Delta^{i,min} \leq p_t^i - p_{t-1}^i \leq \Delta^{i,max}, -\Delta^{j,min} \leq p_t^j - p_{t-1}^j \leq \Delta^{j,max}, \forall t, \forall i \in I_G \cup I_{CHP}, \forall j \in \cup I_{EB} \tag{14}$$

where x_t^i / x_t^j are binary variables and 1 indicates that the unit is in operation; N^i / N^j are the maximum starting times of generator i and CHP i /EB j during the scheduling period; $P^{i,max} / P^{i,min}$ are the maximum/minimum output power of the unit i except EB; $P^{j,max} / P^{j,min}$ are the maximum/minimum output power of EB j ; p_t^j is the output of active

power of EB j ; $\Delta^{i,max} / \Delta^{i,min}$ are the maximum/minimum ramping values of the unit I except EB; and $\Delta^{j,max} / \Delta^{j,min}$ are the maximum/minimum ramping values of EB j .

In addition, the interaction with the grid is constrained by (15), which means that the CHP-VPP cannot buy and sell electricity in one period of time.

$$x_t^{sell} + x_t^{pur} \leq 1, -Mx_t^{pur} \leq p_t^e \leq Mx_t^{sell}, \forall t \tag{15}$$

where M is a very large, positive, real number.

2.3. Operation Constraints of Reconfigurable DHS

The traditional, exact DHS model contains a hydraulic–thermodynamic equation with nonlinear terms and is only applicable to the case where the mass flow direction does not change. Therefore, when solving the CHP-VPP optimal dispatch problem considering DHN reconfiguration, it is essential to convert the exact DHS model into the energy flow model [20]. The core of its transformation is to take the available heat quantity $h_{p,t} = cm_{p,t}(\tau_{p,t}^S - \tau_{p,t}^R)$ in the pipeline as the decision variable and approximate the heat loss.

Similar to the power balance constraint, constraint (16) is the heat balance equation.

$$\sum_{p \in I_j^{P+}} h_{p,t}^{Out} + \sum_{s \in I_j^{HS}} h_{s,t}^{HS} = \sum_{l \in I_j^{HL}} h_{l,t}^{HL} + \sum_{p \in I_j^{P-}} h_{p,t}^{In} \tag{16}$$

where I_j^{HS} , I_j^{HL} represent the sets of heat station and heat load connected to node j ; I_j^{P+} / I_j^{P-} represent the set of pipelines flowing from/to node j ; $h_{p,t}^{In} / h_{p,t}^{Out}$ are the inlet/outlet heat flow of pipeline p ; $m_{p,t}$ is the mass flow of pipeline p ; and $\tau_{p,t}^S / \tau_{p,t}^R$ is the mass flow temperature in pipeline p of the supply/return network.

Constraint (17) indicates that the heat of the heat station comes from the CHP unit and EB.

$$\sum_{i \in I_s^{CHP}} h_t^i + \sum_{j \in I_s^{EB}} h_t^j = h_{s,t}^{HS}, \forall s \in I_{HS}, \forall t \tag{17}$$

where I_s^{EB} , I_s^{CHP} represent the set of EBs and CHP units connected to the heat station s and h_t^j is the heat output of EB j .

Constraints (18) and (19) are limits on the CHP unit, including the limitation of combination factor $\lambda_t^{i,k}$ related to the output of CHP unit i and the limitation of the CHP unit output.

$$0 \leq \lambda_t^{i,k} \leq 1, \sum \lambda_t^{i,k} = x_t^i, \forall k \in OZ^i, \forall t, \forall i \in I_{CHP} \tag{18}$$

$$p_t^{CHP} = \sum_{k \in OZ^i} \lambda_t^{i,k} P^{i,k}, h_t^{CHP} = \sum_{k \in OZ^i} \lambda_t^{i,k} H^{i,k}, \forall t, \forall i \in I_{CHP} \tag{19}$$

where OZ is the set of extreme points in the operation feasible area of CHP unit and $P^{i,k} / H^{i,k}$ are electric/heat power output corresponding to the k -th extreme point, respectively.

Constraint (20) represents the relationship between heat and power output of EB.

$$h_t^{EB} = \lambda^{EB} p_t^{EB}, \forall t \tag{20}$$

where λ^{EB} is the heat–electric coefficient of EB unit.

Constraints (21) and (22) define the meaning of the heat loss and its calculation formula. The heat quality of the pipeline is limited by constraint (23) due to the user’s requirements for the heating temperature.

$$h_{p,t}^{Out} = h_{p,t}^{In} - x_t^p h_{p,t}^{Loss}, \forall p \in I_p, \forall t \tag{21}$$

$$h_{p,t}^{Loss} = \frac{\lambda L}{A\rho} \left(\tau_{p,t}^{In,S,min} + \tau_{p,t}^{In,R,min} - 2\tau_t^{Am} \right), \forall p \in I_p, \forall t \tag{22}$$

$$-x_t^p h_{p,t}^{max} \leq h_{p,t}^{Out}, h_{p,t}^{In} \leq x_t^p h_{p,t}^{max} \tag{23}$$

where x_t^p represents the state of the pipeline p , $h_{p,t}^{Loss}$ is the heat loss of pipeline p , λ is the heat conductivity of the pipeline p , ρ/c are the density/heat capacity of water, L is the length of pipeline p , A is the cross-sectional area of pipeline p , $\tau_{p,t}^{In,S,min} / \tau_{p,t}^{In,R,min}$ represents the minimum inlet temperature of pipeline p in the supply/return network, τ_t^{Am} is the ambient temperature, and $h_{p,t}^{max}$ denotes the upper limit of heat quantity in pipeline p .

Constraint (24) indicates the boundary restraint of unit heat output.

$$x_t^i H^{i,min} \leq h_t^i \leq x_t^i H^{i,max}, x_t^j H^{j,min} \leq h_t^j \leq x_t^j H^{j,max}, \forall t, \forall i \in I_{CHP}, \forall j \in \cup I_{EB} \tag{24}$$

where $H^{i,max} / H^{i,min}$ are the upper and lower limits of the heat output of CHP i and $H^{j,max} / H^{j,min}$ are the upper and lower limits of the heat output of EB j .

The DHN logic constraints (25) and (26) indicate that the total number of pipeline openings before and after reconfiguration cannot change.

$$x_t^p - x_{t-1}^p = a_t^p - b_t^p, \sum_{r=\max\{1,t-T^p+1\}}^t a_r^p \leq x_t^p, \sum_{r=\max\{1,t-T^p+1\}}^t b_r^p \leq 1 - x_t^p \tag{25}$$

$$\sum x_t^p = \sum \tilde{x}_t^p \tag{26}$$

where a_t^p / b_t^p are binary variables representing the opening/closing state of pipeline p , respectively; T^p is the minimum interval time for pipeline operation; and \tilde{x}_t^p is the number of opened pipelines.

2.4. Two-Stage Robust Optimization Model

The above model does not consider the uncertainty of wind farm. Real-time wind output cannot be accurately predicted. Therefore, this paper constructs an adaptive robust optimization (ARO) model considering the uncertainty of wind power, which can be expressed as the following compact form:

$$\begin{aligned} & \min_x a^T x \max_{u \in \Theta^u} \min_y b^T y \\ \text{s.t.} & \begin{cases} Ax = 0, Bx \leq m \\ Cy = 0, Dy \leq n, Ex + Fu + Gy \leq q \end{cases} \end{aligned} \tag{27}$$

where x represents the first-stage variables, containing the start-up states of all devices and the on/off state of valves; u denotes the uncertainty variables, specifically referring to the randomness of the wind output value; y represents the second-stage decision variables, including the electric power and heat output of all devices under confirmed wind generation.

The uncertainty set of wind output Θ^u is as follows, where a robust control coefficient Γ^{WT} is introduced to avoid an over-conservative decision:

$$\begin{aligned} \Theta^u = \{u | & \tilde{p}_t^{WT} = \hat{p}_t^{WT} + (\bar{p}_t^{WT} - \hat{p}_t^{WT}) \cdot b_t^+ - (\hat{p}_t^{WT} - \underline{p}_t^{WT}) \cdot b_t^-, \\ & b_t^+, b_t^- \in [0, 1], \sum_{t=1}^{24} (b_t^+ + b_t^-) \leq \Gamma^{WT} \} \end{aligned} \tag{28}$$

where $\tilde{p}_t^{WT} / \hat{p}_t^{WT}$ are the actual/predicted values of wind power and $\bar{p}_t^{WT} / \underline{p}_t^{WT}$ are the upper and lower limits of wind power.

The value of Γ^{WT} is between 0 and 24, which indicates the maximum number of periods in which the actual wind power generation can fluctuate relative to the predicted value.

3. Solution Methodology

The above ARO model commonly uses C&CG algorithm to effectively deal with the global optimal solution [21]. The algorithm is a method that divides the primary problem into one master problem and one subproblem for iterative solution. The subproblem is used to derive the worst scenario in the uncertainty set; then, the corresponding variables and constraints are introduced to the master problem according to the scenario.

3.1. Master Problem of C&CG

The master problem solves the variables that satisfy the first-stage optimization object according to the worst scenario u_k^* generated by the subproblem.

$$\begin{aligned} \min \quad & a^T x + \eta \\ \text{s.t.} \quad & \eta \geq b^T y_k, \forall k = 1, \dots, n \\ & Ax = 0, Bx \leq m \\ & Cy_k = 0, Dy_k \leq n, Ex + Fu_k^* + Gy_k \leq q \end{aligned} \tag{29}$$

3.2. Subproblem of C&CG

According to the optimal first-stage decision variables, the subproblem solves the max–min model to obtain the worst scenario u_k^* and the optimal object value.

$$\begin{aligned} \eta(x^*, u, y) = \max_{u \in \Theta^u} \min_y \quad & b^T y \\ \text{s.t.} \quad & Cy = 0 \\ & Dy \leq n \\ & Ex + Fu + Gy \leq q \end{aligned} \tag{30}$$

In summary, the solving steps of the CHP-VPP two-stage robust optimization are as follows:

- (1) Initialize the iteration number $n = 0$ and set the bounds of the model $UB = +\infty, LB = -\infty$.
- (2) Solve the master problem and obtain the optimal solution x^* and η^* . Update $LB = \max\{LB, a^T x^* + \eta^*\}$.
- (3) Solve the subproblem with x^* ; derive the uncertain scenario parameter u^* and the optimal solution y^* . Update $UB = \min\{UB, a^T x^* + \eta(x^*, u^*, y^*)\}$.
- (4) If $UB - LB \leq \epsilon$, quit the iteration. Otherwise, update the worst scenario in the master problem, then go to (2).

The specific flow chart of the above C&CG algorithm is shown in Figure 2.

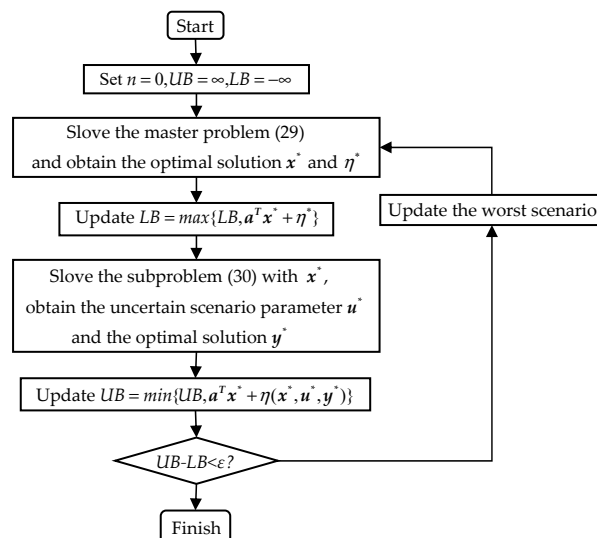


Figure 2. C&CG algorithm flow chart.

4. Case Studies

All tests are resolved using CPLEX interfaced through MATLAB [22].

4.1. Test System Description

Figure 3 depicts the test system selected in this paper. The test system is composed of a 33-node PDS and 8-node DHS, referred to as the P33H8 system. Heating is provided by two heat stations (denoted as HS1 and HS2) in the DHS to satisfy the heat demand. HS1 consists of one EB and one extraction–condensing CHP unit (CHP1), while HS2 is equipped with only one backpressure CHP unit (CHP2). Under normal conditions, the valve v5 is closed and other valves are open, HL3 is supplied by HS2, and HL1 and HL2 are distributed to HS1.

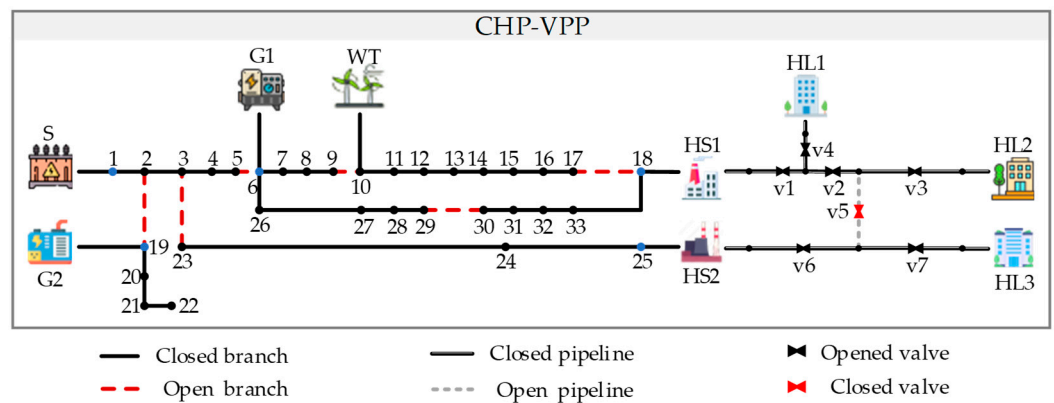


Figure 3. Configuration of the P33H8 system.

4.2. Scenario Settings and Results Analysis

The following three cases are investigated to compare and analyze the results:

Case 1: neither the reconfigurability of DHN nor the uncertainty of wind power are taken into account, i.e., the valve v5 is normally closed, and the output of wind power is its predicted value.

Case 2: the reconfiguration of the DHN is achieved by remote control of the sectionalizing and tie valves, but the fluctuation of wind power is still ignored.

Case 3: both the reconfigurability of DHN and the uncertainty of wind power are discussed. The total costs in Case 1 to Case 3 are displayed in Table 1.

Table 1. Costs and revenues in Case 1 to Case 3.

| | C^s | C^f | C^e | Total Cost |
|--------|-------|-----------|-----------|------------|
| Case 1 | 6400 | 72,925.94 | 7954.03 | 87,279.97 |
| Case 2 | 6400 | 64,158.62 | 14,295.77 | 84,854.39 |
| Case 3 | 6400 | 64,158.62 | 17,547.05 | 88,105.67 |

4.2.1. Analysis of DHN Reconfiguration

The tie-line power between the CHP-VPP and grid of Case 1 (i.e., ignoring the reconfigurability of DHN) and Case 2 (i.e., considering the DHN reconfiguration) are shown in Figure 4.

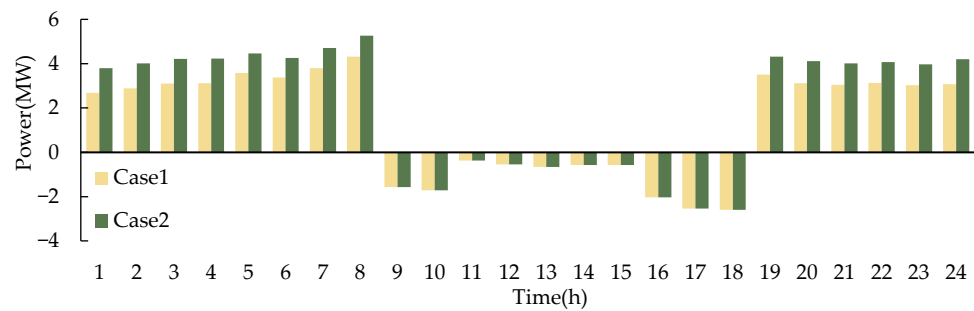


Figure 4. The tie-line power between the CHP-VPP and grid of Case 1 and Case 2.

(1) Ignoring the reconfigurability of DHN

At this time, the value v5 often remains closed, HL1 and HL2 are heated by HS1 and HL3 is heated by HS2. Figure 5a is the output curve of each unit in Case 1.

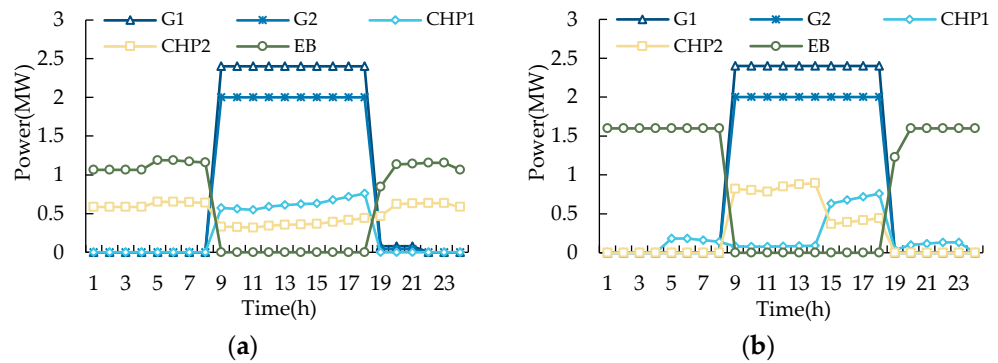


Figure 5. Output curve of each unit: (a) Case 1; (b) Case 2.

Before 8:00 and after 19:00, HS1 is basically heated by EB, which is due to the lower electricity price during these periods, as it is more economical to purchase electricity from the power grid than to start CHP units for power generation. The output of CHP2 is confirmed by HL3; during 9:00 to 18:00, due to the rise in electricity prices, the output of CHP units is increased to sell more electricity to the grid to earn more revenue. The EB unit is shut down owing to its power consumption properties.

(2) Considering the reconfigurability of DHN

After considering the reconfigurability of DHN, the heat load will be redistributed among the participating heat sources so that the output of each heating unit can be flexibly changed to seek the most economical scheduling plan. As compared with Case 1, the total costs decrease by 2.78% in Case 2. Figure 5b is the output curve of each unit in Case 2. Figure 6 shows different topologies of DHN under reconfiguration operation in Case 2.

During 0:00 to 8:00 and 19:00 to 24:00, the load originally heated by CHP2 in Case 1 can be heated by the less-expensive EB unit since the DHN can be reconfigured. At this time, the value v6 is turned off and all heat loads are supplied by HS1. It can be seen from Figure 5 that the output of CHP2 is reduced, while the EB unit operates at maximum power. When EB cannot meet all the heat load, the CHP1 unit starts to meet the remaining heat load. Therefore, the quantity of electricity purchased from the grid during these periods is higher than in Case 1; from 9:00 to 14:00, the cheaper CHP2 unit provides the heat originally borne by CHP1 in Case 1 to reduce costs; from 15:00 to 18:00, the output of wind power increases significantly. The CHP1 unit with a wider operating range is selected to increase its output and absorb more wind power, while the output of the CHP2 unit is relatively reduced. At this point, the valve v5 is turned off so that HL1 and HL2 are provided by HS1, while HL3 is provided by HS2.

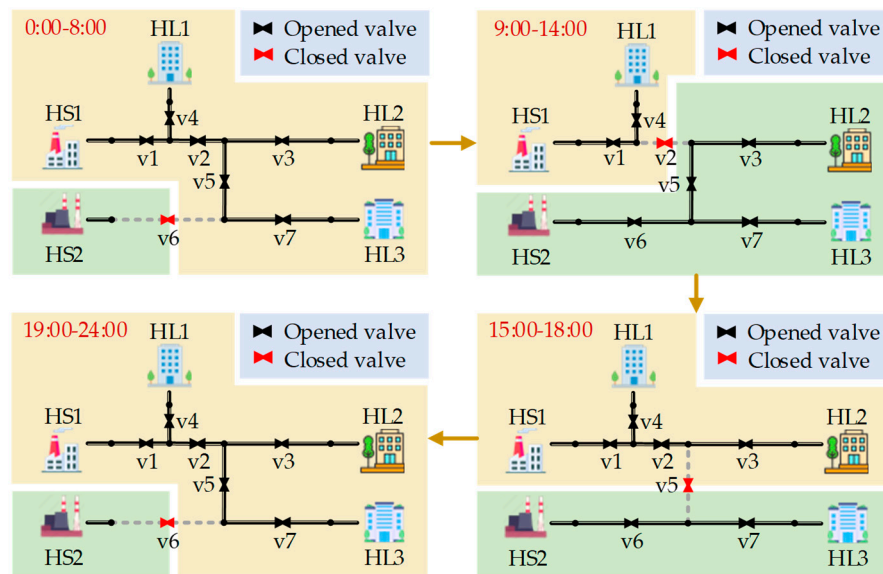


Figure 6. Network topology of different time periods in Case 2.

4.2.2. Analysis of Uncertainty of Wind Power

The wind power value in Case 2 is a certain predicted value, while its output in Case 3 is random and $\Gamma^{WT} = 12$ (i.e., the wind power output can take the maximum or minimum value of the fluctuation interval in 12 periods). Figure 7 displays the wind power output values in Case 2 and Case 3, respectively. Figure 8 shows the tie-line power between the CHP-VPP and grid of Case 2 (i.e., ignoring the uncertainty of wind power) and Case 3 (i.e., considering the uncertainty of wind power).

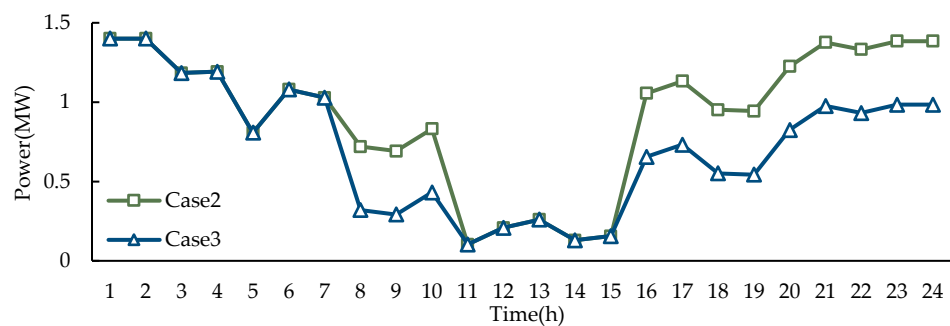


Figure 7. The wind power output values in Case 2 and Case 3.

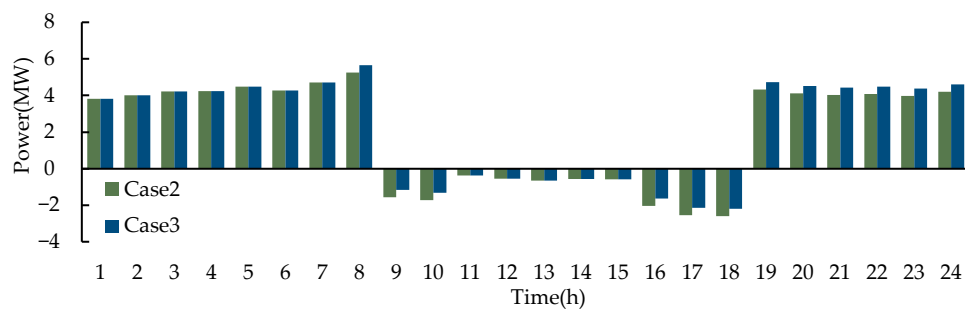


Figure 8. The tie-line power between the CHP-VPP and grid of Case 2 and Case 3.

The worst scenario of the model is that the wind power takes the minimum value of the fluctuation range from Figure 7. Meanwhile, the CHP-VPP needs to buy more electricity from the power grid when the electricity price is low. When the electricity price is high, due

to the reduction in wind power output, the quantity of electricity sold by the CHP-VPP to the power grid also decreases accordingly. This leads to an increase in electricity purchase costs, a decrease in electricity sales revenue and, ultimately, a significant increase in the total cost of CHP-VPP.

By adjusting the value of the robustness coefficient, different robustness optimization results can be obtained. The robustness coefficient reflects the ability of the decision-making scheme to resist risks and directly affects the scheduling scheme [23]. Figure 9 shows the total cost of the CHP-VPP under different robustness coefficients.

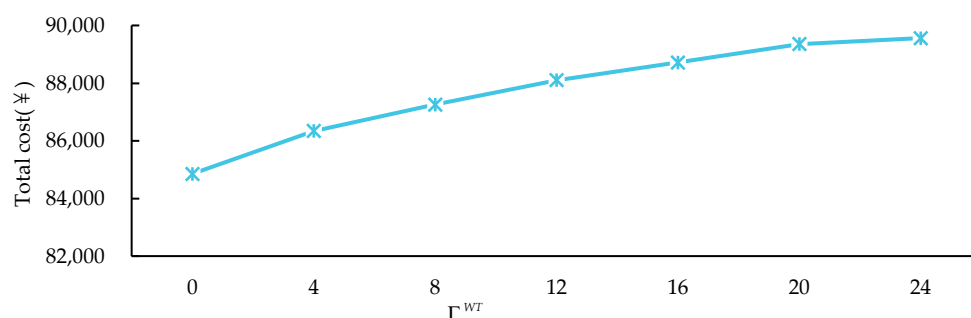


Figure 9. The total cost of the CHP-VPP under different robustness coefficients.

4.2.3. Results of an Actual CHP-VPP in Beijing, China

The actual CHP-VPP in Beijing includes a 7-node PDS and 11-node DHS [24], equipped with three CHP units, one gas boiler and three WTs. Among them, HS2 (connected to node 2) and HS3 (connected to node 6) are provided by one CHP unit, respectively, and HS1 (connected to node 1) includes a CHP unit and a gas boiler. The heat load is connected at nodes 7, 8, 9, 10 and 11. The total cost of Case 1 and Case 2 in the system is shown in Table 2.

Table 2. Costs and revenues in Case 1 and Case 2 in the actual CHP-VPP.

| | C^s | C^f | C^e | Total Cost |
|--------|-------|-----------|------------|------------|
| Case 1 | 5400 | 89,103.77 | −15,513.90 | 78,989.87 |
| Case 2 | 5400 | 88,698.03 | −14,197.65 | 75,040.38 |

The total cost of Case 2 is 5.00% lower than that of Case 1 from Table 2, which shows that by redistributing heat load between different heat stations, the heat generation of CHP units can be adjusted more flexibly and the flexibility of the power system can be improved effectively.

5. Conclusions

A CHP-VPP optimal dispatch model considering the reconfigurability of DHN and its optimal operation strategy is proposed in this paper, which significantly reduces the total cost of the park-level CHP-VPP. At the same time, ARO is used to tackle with the randomness of wind power, which enhances the robustness of operation. According to the different risk preferences of operators, different robust coefficients are selected for scheduling schemes.

This paper concentrates on the operation optimization of CHP-VPP. The operation optimization of CHP-VPP considering coordinated reconfiguration of integrated power distribution and heating networks under multi-dimensional uncertainty can be studied in the future.

Author Contributions: Conceptualization, J.W.; Supervision, J.W. and B.W.; Project administration, J.W., G.Y. and S.L.; Methodology, Z.P. and H.G.; Writing—original draft, Z.P. and H.G.; Writing—review & editing, Z.P., H.G. and B.W.; Validation, S.L. and G.Y.; Investigation, S.L. All authors have read and agreed to the published version of the manuscript.

Funding: This research is funded by the Science and Technology Project of Shanxi Electric Power Company No. 52053022000K.

Data Availability Statement: Not applicable.

Conflicts of Interest: The authors declare no conflict of interest.

References

1. Li, Y. New energy utilization in environmental design and realization. *Energy Rep.* **2022**, *8*, 9211–9220.
2. Ghiasi, M. Detailed study, multi-objective optimization, and design of an AC-DC smart microgrid with hybrid renewable energy resources. *Energy* **2019**, *169*, 496–507. [[CrossRef](#)]
3. Renewable Capacity Highlights. 2020. Available online: <https://www.irena.org/statistics> (accessed on 2 June 2020).
4. Jamali, A.; Aghaei, J.; Esmaili, M.; Nikoobakht, A.; Niknam, T.; Shafie-Khah, M.; Catalao, J.P.S. Self-scheduling approach to coordinating wind power producers with energy storage and demand response. *IEEE Trans. Sustain. Energy* **2020**, *11*, 1210–1219. [[CrossRef](#)]
5. Li, B.; Ghiasi, M. A new strategy for economic virtual power plant utilization in electricity market considering energy storage effects and ancillary services. *J. Electr. Eng. Technol.* **2021**, *16*, 2863–2874. [[CrossRef](#)]
6. Li, J.; Zhu, Y.; Yong, M. Cooperative operation and profit distribution of virtual power plant. *Electr. Power Compon. Syst.* **2023**, *51*, 71–82. [[CrossRef](#)]
7. Yang, X.; Niu, D.; Sun, L.; Wang, K.; De, G. Participation of electric vehicles in auxiliary service market to promote renewable energy power consumption: Case study on deep peak load regulation of auxiliary thermal power by electric vehicles. *Energy Sci. Eng.* **2021**, *9*, 1465–1476. [[CrossRef](#)]
8. Tan, Z.; Zhong, H.; Xia, Q.; Kang, C.; Wang, X.S.; Tang, H. Estimating the robust P-Q capability of a technical virtual power plant under uncertainties. *IEEE Trans. Power Syst.* **2020**, *35*, 4285–4296. [[CrossRef](#)]
9. Kardakos, E.G.; Simoglou, C.K.; Bakirtzis, A.G. Optimal offering strategy of a virtual power plant: A stochastic bi-level approach. *IEEE Trans. Smart Grid* **2016**, *7*, 794–806. [[CrossRef](#)]
10. Wang, S.; Wu, W. Aggregate flexibility of virtual power plants with temporal coupling constraints. *IEEE Trans. Smart Grid* **2021**, *12*, 5043–5051. [[CrossRef](#)]
11. Mohsen Hosseini, S.; Carli, R.; Jantzen, J.; Dotoli, M. Multi-block ADMM approach for decentralized demand response of energy communities with flexible loads and shared energy storage system. In Proceedings of the 2022 30th Mediterranean Conference on Control and Automation (MED), Vouliagmeni, Greece, 28 June–1 July 2022; pp. 67–72.
12. Ancona, M.A.; Baldi, F.; Branchini, L.; De Pascale, A.; Gianaroli, F.; Melino, F.; Ricci, M. Comparative analysis of renewable energy community designs for district heating networks: Case study of corticella (Italy). *Energies* **2022**, *15*, 5248. [[CrossRef](#)]
13. Daniel, F.; Erik, M.; Russell, M.; Ute, K.; Wolf, F. On the economic potential for electric load management in the German residential heating sector—An optimizing energy system model approach. *Energy* **2014**, *71*, 263–276.
14. Fang, F.; Yu, S.; Liu, M. An improved Shapley value-based profit allocation method for CHP-VPP. *Energy* **2020**, *213*, 118805. [[CrossRef](#)]
15. Kordestani, M.; Zanj, A.M.; Orchard, E.; Saif, M. A modular fault diagnosis and prognosis method for hydro-control valve system based on redundancy in multisensory data information. *IEEE Trans. Reliab.* **2019**, *68*, 330–341. [[CrossRef](#)]
16. Du, Y.; Xue, Y.; Wu, W.; Shahidehpour, M.; Shen, X.; Wang, B.; Sun, H. Coordinated planning of integrated electric and heating system considering the optimal reconfiguration of district heating network. *IEEE Trans. Power Syst.* **2023**, 1–14. [[CrossRef](#)]
17. Wang, K.; Xue, Y.; Guo, Q.; Shahidehpour, M.; Zhou, Q.; Wang, B.; Sun, H. A coordinated reconfiguration strategy for multi-stage resilience enhancement in integrated power distribution and heating networks. *IEEE Trans. Smart Grid* **2022**, *14*, 2709–2722. [[CrossRef](#)]
18. Zhao, H.; Wang, B.; Pan, Z.; Sun, H.; Guo, Q.; Xue, Y. Aggregating additional flexibility from quick-start devices for multi-energy virtual power plants. *IEEE Trans. Sustain. Energy* **2021**, *12*, 646–658. [[CrossRef](#)]
19. Yeh, H.-G.; Gayme, D.F.; Low, S.H. Adaptive VAR control for distribution circuits with photovoltaic generators. *IEEE Trans. Power Syst.* **2012**, *27*, 1656–1663. [[CrossRef](#)]
20. Xue, Y.; Shahidehpour, M.; Pan, Z.; Wang, B.; Zhou, Q.; Guo, Q.; Sun, H. Reconfiguration of district heating network for operational flexibility enhancement in power system unit commitment. *IEEE Trans. Sustain. Energy* **2021**, *12*, 1161–1173. [[CrossRef](#)]
21. Zeng, B.; Zhao, L. Solving two-stage robust optimization problems using a column-and-constraint generation method. *Oper. Res. Lett.* **2013**, *41*, 457–461. [[CrossRef](#)]
22. Hong, T.; Zhao, D.; Zhang, Y.; Cui, B.; Tian, Y. Optimal voltage reference for droop-based DERs in distribution systems. *IEEE Trans. Smart Grid* **2020**, *11*, 2357–2366. [[CrossRef](#)]
23. Baringo, A.; Baringo, L.; Arroyo, J.M. Day-ahead self-scheduling of a virtual power plant in energy and reserve electricity markets under uncertainty. *IEEE Trans. Power Syst.* **2019**, *34*, 1881–1894. [[CrossRef](#)]
24. Qin, X.; Shen, X.; Guo, Y.; Pan, Z.; Guo, Q.; Sun, H. Combined electric and heat system testbeds for power flow analysis and economic dispatch. *CSEE J. Power Energy Syst.* **2021**, *7*, 34–44.

Disclaimer/Publisher’s Note: The statements, opinions and data contained in all publications are solely those of the individual author(s) and contributor(s) and not of MDPI and/or the editor(s). MDPI and/or the editor(s) disclaim responsibility for any injury to people or property resulting from any ideas, methods, instructions or products referred to in the content.